Mechanism and Quantum Mechanical Tunneling Effects on Inner Hydrogen Atom Transfer in Free Base Porphyrin: A Direct ab Initio Dynamics Study

ARTICLE *in* JOURNAL OF THE AMERICAN CHEMICAL SOCIETY · JANUARY 2000

Impact Factor: 12.11 · DOI: 10.1021/ja9925094

3 AUTHORS, INCLUDING:

Thanh Truong
University of Utah
168 PUBLICATIONS **6,145** CITATIONS

SEE PROFILE

Mechanism and Quantum Mechanical Tunneling Effects on Inner Hydrogen Atom Transfer in Free Base Porphyrin: A Direct ab Initio Dynamics Study

Dilip K. Maity,† Robert L. Bell, and Thanh N. Truong*

Contribution from the Henry Eyring Center for Theoretical Chemistry, Department of Chemistry, University of Utah, Salt Lake City, Utah 84112

Received July 15, 1999. Revised Manuscript Received October 15, 1999

Abstract: A theoretical study of the mechanism and kinetics of the inner double hydrogen atom-transfer process in free base porphyrin is presented. Our analysis reveals that the stepwise mechanism first requires the porphyrin ring to compress at an approximate cost of 8.7 kcal/mol, followed by transfer of a H atom with an additional energy requirement of 8.2 kcal/mol. Solvent effects were investigated using a dielectric continuum model and found to be small. The forward and reverse rate constants for the hydrogen atom-transfer process of trans-isomer ↔ cis-isomer were calculated using a canonical variational transition-state theory augmented by multidimensional semiclassical tunneling approximations in the temperature range of 200−1000 K. The calculated activation energy of 10.8 kcal/mol in the temperature range of 200−300 K agrees well with the available experimental data. We found that tunneling is significant for both the forward and reverse trans ↔ cis tautomerization processes, especially in the low-temperature range.

Introduction

Free base porphyrin has two hydrogen atoms in the inner part of the skeleton. It is known that the two inner hydrogen atoms migrate in a framework of four nitrogen sites, and the process is known as NH tautomerization. This process is significantly important in photosynthesis and metal coordination chemistry. Furthermore, porphyrins have been used in designing advanced materials such as organic metals, molecular wires, and other devices and in medicine for the treatment of cancer and dermatological diseases. Due to these potential practical applications, the mechanism of the NH tautomerization in free base porphyrin has attracted considerable experimental[1−24] and theoretical[25−42] interest. There are two proposed mechanisms for this tautomerization: stepwise[2,13,15−18,31] and concerted.[3,4,27,32,33] The stepwise mechanism is characterized by a trans−cis−trans conversion, with the trans-isomer as the reactant and the cis-isomer as the intermediate. This involves the migration of the

* Corresponding author.
† On leave from Chemistry Division, Bhabha Atomic Research Centre, Bombay, India.

(1) Chen, B. M. L.; Tulinsky, A. *J. Am. Chem. Soc.* **1972**, *94*, 4144.
(2) Abraham, R. J.; Hawkes, G. E.; Smith, K. M. *Tetrahedron Lett.* **1974**, *16*, 1483.
(3) Eaton, S. S.; Eaton, G. R. *J. Am. Chem. Soc.* **1977**, *99*, 1601.
(4) Hennig, J.; Limbach, H.-H. *J. Chem. Soc., Faraday Trans. 2* **1979**, *75*, 752.
(5) Limbach, H.-H.; Hennig, J.; Gerritzen, D.; Rumpel, H. *Faraday Discuss. Chem. Soc.* **1982**, *74*, 229.
(6) Hennig, J.; Limbach, H.-H. *J. Magn. Reson.* **1982**, *49*, 322.
(7) Hennig, J.; Limbach, H.-H. *J. Am. Chem. Soc.* **1984**, *106*, 292.
(8) Limbach, H.-H.; Hennig, J.; Kendrick, R.; Yannov, C. S. *J. Am. Chem. Soc.* **1984**, *106*, 4059.
(9) Crossley, M. J.; Harding, M. M.; Sternhell, S. *J. Am. Chem. Soc.* **1986**, *108*, 3608.
(10) Schlabach, M.; Wehrle, B.; Limbach, H.-H.; Bunnenberg, E.; Knierzinger, A.; Shu, A. Y. L.; Tolf, B. R.; Djerassi, C. *J. Am. Chem. Soc.* **1986**, *108*, 3856.
(11) Stilbs, P.; Moseley, M. E. *J. Chem. Soc., Faraday Trans. 2* **1980**, *76*, 729.
(12) Stilbs, P. *J. Magn. Reson.* **1984**, *58*, 152.
(13) Schlabach, M.; Scherer, G.; Limbach, H.-H. *J. Am. Chem. Soc.* **1991**, *113*, 3550.
(14) Braun, J.; Schlabach, M.; Wehrle, B.; Köcher, M.; Vogel, E.; Limbach, H.-H. *J. Am. Chem. Soc.* **1994**, *116*, 6593.
(15) Braun, J.; Limbach, H.-H.; Williams, P. G.; Morimoto, H.; Wemmer, D. E. *J. Am. Chem. Soc.* **1996**, *118*, 723.
(16) Limbach, H.-H.; Hennig, J.; Stulz, J. *J. Chem. Phys.* **1983**, *78*, 5432.
(17) Frydman, L.; Olivieri, A. C.; Diaz, L. E.; Frydman, B.; Morin, F. G.; Mayne, C. L.; Grant, D. M.; Adler, A. D. *J. Am. Chem. Soc.* **1988**, *110*, 336.
(18) Butenhoff, T. J.; Moore, C. B. *J. Am. Chem. Soc.* **1988**, *110*, 8336.
(19) Butenhoff, T. J.; Chuck, R. S.; Limbach, H.-H.; Moore, C. B. *J. Phys. Chem.* **1990**, *94*, 7847.
(20) Spiro, T. G. *Adv. Protein Chem.* **1985**, *37*, 111.
(21) Yu, N.-T. *Methods Enzymol.* **1986**, *130*, 350.
(22) Spiro, T. G. *Biological Applications of Raman Spectroscopy*; Wiley-Interscience: New York, 1988; Vol. 3.
(23) Radziszewski, J. G.; Waluk, J.; Michl, J. *J. Chem. Phys.* **1989**, *136*, 165.
(24) Radziszewski, J. G.; Waluk, J.; Michl, J. *J. Mol. Spectrosc.* **1990**, *140*, 373.
(25) Li, X.-Y.; Zgierski, M. Z. *J. Phys. Chem.* **1991**, *95*, 4268.
(26) Almlöf, J. *Int. J. Quantum Chem.* **1974**, *8*, 152.
(27) Limbach, H.-H.; Hennig, J. *J. Chem. Phys.* **1979**, *71*, 3120.
(28) Sarai, A. *J. Chem. Phys.* **1984**, *80*, 5341.
(29) Kuzmitsky, V. A.; Solovyov, K. N. *J. Mol. Struct.* **1980**, *65*, 219.
(30) Sarai, A. *Chem. Phys. Lett.* **1981**, *83*, 50.
(31) Sarai, A. *J. Chem. Phys.* **1982**, *76*, 5554.
(32) Merz, K. M. J.; Reynolds, C. H. *J. Chem. Soc., Chem. Commun.* **1988**, 90.
(33) Smedarchina, Z.; Siebrand, W.; Wildman, T. A. *Chem. Phys. Lett.* **1988**, *143*, 395.
(34) Almlöf, J.; Fischer, T. H.; Gassman, P. G.; Ghosh, A.; Häser, M. *J. Phys. Chem.* **1993**, *97*, 10964.
(35) Ghosh, A.; Almlöf, J. *Chem. Phys. Lett.* **1993**, *213*, 519.
(36) Ghosh, A. *J. Phys. Chem.* **1994**, *98*, 11004.
(37) Merchàn, M.; Ortí, E.; Roos, B. O. *Chem. Phys. Lett.* **1994**, *221*, 136.
(38) Reimers, J. R.; Lü, T. X.; Crossley, M. J.; Hush, N. S. *J. Am. Chem. Soc.* **1995**, *117*, 2855.
(39) Ghosh, A.; Almlöf, J. *J. Phys. Chem.* **1995**, *99*, 1073.
(40) Kozlowski, P. M.; Zgierski, M. Z.; Pulay, P. *Chem. Phys. Lett.* **1995**, *247*, 379.
(41) Kozlowski, P. M.; Jarzecki, A. A.; Pulay, P. *J. Phys. Chem.* **1996**, *100*, 7007.
(42) Baker, J.; Kozlowski, P. M.; Jarzecki, A. A.; Pulay, P. *Theor. Chem. Acc.* **1997**, *97*, 59.

10.1021/ja9925094 CCC: $19.00
Published on Web 01/19/2000

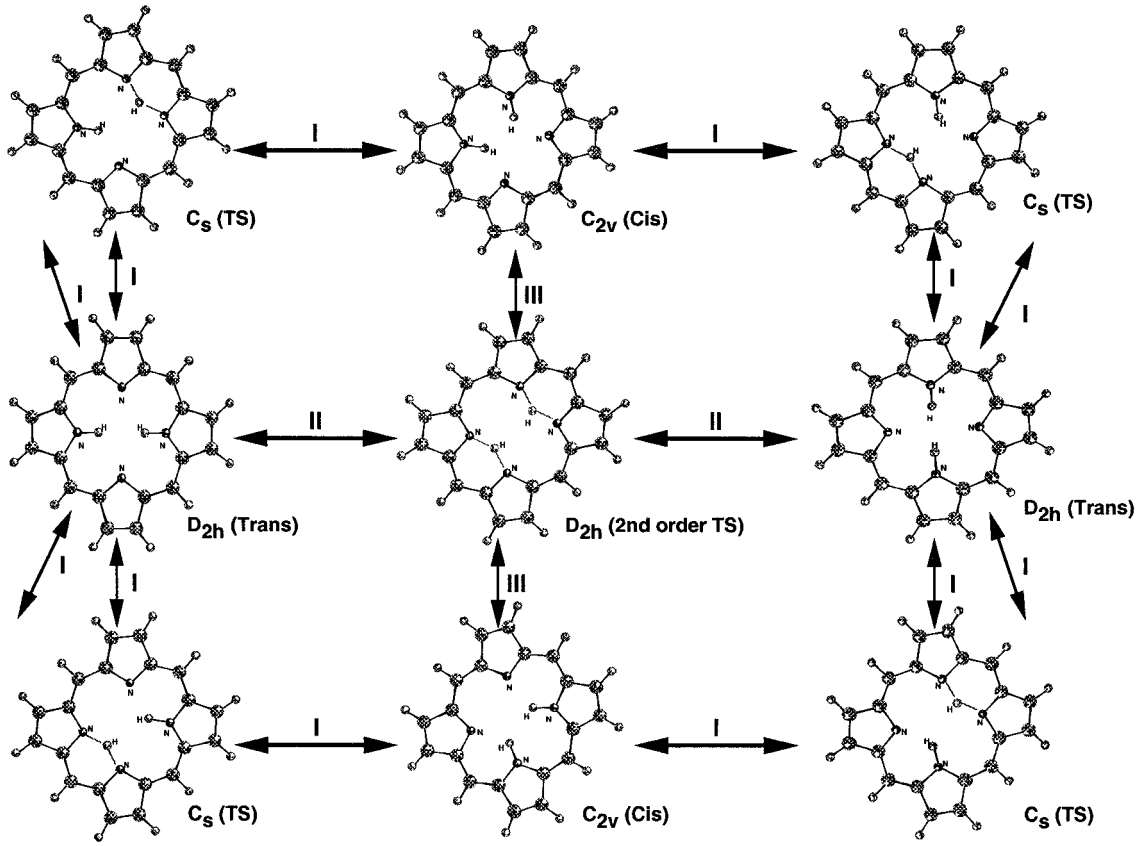

Figure 1. Schematic diagram of the inner hydrogen tautomerization process of free base porphyrin. Path I describes the stepwise mechanism, and path II describes the concerted mechanism. Path III connects the second-order saddle point geometry to the intermediate geometry. The symmetry of each stationary point is also shown.

two hydrogen atoms one after another as shown in path I of Figure 1. The concerted mechanism involves synchronous migration of both H atoms as shown in path II of Figure 1. Debate as to whether the mechanism is stepwise or concerted extends back many years for both experiment and theory. It is now generally accepted both theoretically[30,32,34,37−42] and experimentally[14,15,17−19] that the double proton transfer occurs via a two-step mechanism involving a metastable cis intermediate rather than by a synchronous one-step path. The rate of tautomerization for the stepwise mechanism as a function of temperature has been measured using dynamic liquid-state ^{1}H NMR spectroscopy.[15]

Previously there has been some discussion regarding the structure of the reactant as to whether it is of C_{2v} or D_{2h} symmetry. RHF geometry optimization[39] yields bond-alternating frozen resonance structures of C_{2v} symmetry. It has been hypothesized that a rapid equilibrium occurs between these two structures.[38] Inclusion of electron correlation yields the higher symmetry (D_{2h}) structure as reported by Almlöf and co-workers from their local density functional theory (LDA) and MP2/DZP2 calculations.[34] This prediction has been verified using multireference wave functions[37] and nonlocal hydrid density functional[40] calculations and is consistent with the experimental data. Structural data from X-ray,[1] Raman, and IR[20−25] experiments suggest that the reactant has D_{2h} symmetry. Recently, Baker and co-workers characterized all the stationary points for both stepwise and concerted mechanisms using the hybrid B3-LYP exchange correlation functional with the triple-ζ double-polarization (TZ2P) basis set.[42] This is perhaps the most complete investigation of the mechanism of this reaction to date. They have also reported the NH tautomerization rate from conventional transition-state theory (TST) calculations without any tunneling correction. It is known that double hydrogen atom transfer with a noticeable barrier, such as in this reaction, would have significant tunneling effects, even at room temperature. For example, at room temperature tunneling enhances the rate by a factor of 200 in the double hydrogen atom transfer in the formamidine−water complex.[43,44] However, to accurately account for the tunneling effects would require one to go beyond the conventional TST method.

The main objectives of this study are to address three important issues that have not been considered previously. First is a closer look at how the structure of porphyrin changes as it proceeds from the reactant to the intermediate in the preferred stepwise mechanism. This is done by determining the minimum energy path connecting the trans- and cis-isomers. Second is the magnitude of solvent effects on the energetics of this reaction. Here we employed a dielectric continuum model with a molecular-shaped cavity to estimate the free energies of solvation of porphyrin in heptane, toluene, and methanol. Third is the importance of quantum mechanical tunneling. This was done by employing a direct dynamics method.

Tunneling effects in a system of this size are particularly challenging for several reasons. First, an analytical potential energy function for this process is not available, and the conventional approach of reactive dynamic calculations is not viable. Thus, direct dynamics approaches provide a viable alternative where all the potential energy surface information along the minimum energy path required for evaluating dynamic properties is obtained directly from electronic structure calculations rather than from empirical analytical force fields. The direct

(43) Bell, R. L.; Truong, T. N. *J. Chem. Phys.* **1994**, *101*, 10442.
(44) Bell, R. L.; Taveras, D. L.; Truong, T. N.; Simons, J. *Int. J. Quantum Chem.* **1997**, *63*, 861.

dynamics approach based on a reaction path Hamiltonian methodology such as the variational transition-state theory (VTST) would be preferred since, within the VTST framework, several rather accurate multidimensional semiclassical tunneling methods can be utilized.[45−53]

In the present study, we employed a direct ab initio dynamics method[43,51−53] developed in our laboratory to obtain thermal rate constants for inner-hydrogen atom transfer in free base porphyrin at the level of canonical variational transition-state theory (CVT) augmented by multidimensional semiclassical tunneling methods. Although experimental studies of the NH tautomerization in porphyrin were done in solutions of different solvents and in the solid state, it was found that the condensed-phase effects are small.[14,17] This is, in fact, confirmed theoretically in this study, as discussed below. Thus, it is possible to model the kinetics of this process in the gas phase. Due to the size of the porphyrin, computational demand for CVT rate calculations is enormous. To make this study possible, the present dynamical method utilizes an advanced focusing technique[53] to optimize the cost per performance ratio, i.e., minimizing the number of electronic structure calculations while maintaining the desired level of accuracy. In addition, the combination of Becke's half-and-half (BH&H)[54] exchange with Lee−Yang−Parr (LYP)[55] correlation functionals was used to calculate the potential energy information needed for rate determination, namely geometries, gradients, and Hessians at the stationary points and at selected points along the minimum energy path (MEP). This particular nonlocal hybrid density functional has been shown to give rather accurate transition-state properties in previous studies of water-assisted tautomerization systems.[44,56] Thus, we expect its performance is similar for this reaction. However, to confirm it we have also carried out single-point energy calculations using the integrated molecular orbital + molecular orbital (IMOMO) method recently proposed by Morokuma and co-workers.[57−60]

Theory

I. Variational Transition-State Theory. The variational transition-state rate constants for a gas-phase unimolecular reaction are determined by varying the location of the dividing surface along a reference path to minimize the rate, so as to minimize the error due to "recrossing" trajectories.[61−63] The reference path is the minimum energy path (MEP), which is defined as the steepest descent path from the saddle point to both the reactant and product sides in the mass-weighted Cartesian coordinate system. The reaction coordinate, s, is defined as the distance along the MEP with the origin located at the saddle point and is positive on the product side and negative on the reactant side. For a canonical ensemble at a given temperature T, the canonical variational theory (CVT) thermal rate constant is given by

$$k^{\mathrm{CVT}}(T,s) = \min_{s}\{k^{\mathrm{GT}}(T,s)\} \tag{1}$$

where

$$k^{\mathrm{CVT}}(T,s) = \left\{\sigma\frac{k_{\mathrm{B}}T}{h}\frac{Q^{\mathrm{GT}}(T,s)}{\Phi^{\mathrm{R}}(T)}e^{-V_{\mathrm{MEP}}(s)/k_{\mathrm{b}}T}\right\} \tag{2}$$

In these equations, $k^{\mathrm{GT}}(T,s)$ is the generalized transition-state theory rate constant at the dividing surface which intersects the MEP at s and is orthogonal to the MEP at the intersection point. Q^{GT} is the internal partition function of the generalized transition state with the local zero of energy at $V_{\mathrm{MEP}}(s)$, which is the classical potential energy along the minimum energy path at s with its zero of energy at the reactants. Φ^{R} is the reactant partition function. σ is the symmetry factor accounting for the possibility of more than one symmetry-related reaction path. In the present case, $\sigma = 4$ (see Figure 1) for the forward reaction (trans → cis) and $\sigma = 2$ for the reverse reaction (cis → trans). k_{B} is Boltzman's constant; h is Plank's constant. Both Q^{GT} and Φ^{R} are approximated as products of electronic, rotational, and vibrational partition functions. The vibrational and rotational partition functions were calculated quantum mechanically within the harmonic and rigid rotor approximations, respectively. To include the quantum mechanical effects for motion along the reaction coordinate, CVT rate constants (k^{CVT}) are multiplied by a temperature-dependent transmission coefficient, $\kappa(T)$. This coefficient accounts for both the nonclassical reflection when the total energy of the system is above the barrier and the tunneling effects when the energy is below the threshold barrier. The final rate constant is given by

$$k(T) = \kappa(T)k^{\mathrm{CVT}}(T) \tag{3}$$

II. Semiclassical Tunneling Methods. The effective potential for tunneling is approximated as the vibrational adiabatic ground-state potential, which has the form

$$V_{\mathrm{a}}^{\mathrm{G}}(s) = V_{\mathrm{MEP}}(s) + \sum_{i=1}^{3N-7}\frac{1}{2}h\omega_i(s) \tag{4}$$

At the TST level of rate calculation, where the potential energy surface information is available only at the stationary points, the Wigner (W) and zeroth-order interpolation zero-curvature tunneling (ZCT-0) methods have been applied to calculate the respective transmission coefficients. The ZCT-0 approximation is also known as the Eckart tunneling model.[64] In this model, $V_{\mathrm{a}}^{\mathrm{G}}(s)$ and $V_{\mathrm{MEP}}(s)$ are represented by Eckart functions, whose parameters are determined from fitting to energetic information at the stationary points. More accurate treatments of tunneling effects require more potential energy information. Within the CVT framework, the transmission coefficients can be calculated with multidimensional semiclassical zero and small-curvature tunneling methods,[65,66] denoted as ZCT and SCT, respectively, and were done in this study. The SCT transmission coefficients, which include the reaction path curvature effect on the transmission probability, are based on the centrifugal dominant small-curvature approximation.[66] In

(45) Truhlar, D. G.; Gordon, M. S. *Science* **1990**, *249*, 491.
(46) Gonzalezlafont, A.; Truong, T. N.; Truhlar, D. G. *J. Chem. Phys.* **1991**, *95*, 8875.
(47) Gonzalezlafont, A.; Truong, T. N.; Truhlar, D. G. *J. Phys. Chem.* **1991**, *95*, 4618.
(48) Nguyen, K. A.; Rossi, I.; Truhlar, D. G. *J. Chem. Phys.* **1995**, *103*, 5522.
(49) Corchado, J. C.; Espinosagarcia, J.; Hu, W. P.; Rossi, I.; Truhlar, D. G. *J. Phys. Chem.* **1995**, *99*, 687.
(50) Chuang, Y. Y.; Truhlar, D. G. *J. Phys. Chem. A* **1997**, *101*, 3808.
(51) Truong, T. N. *J. Chem. Phys.* **1994**, *100*, 8014.
(52) Truong, T. N.; Duncan, W. T. *J. Chem. Phys.* **1994**, *101*, 7408.
(53) Duncan, W. T.; Bell, R. L.; Truong, T. N. *J. Comput. Chem.* **1998**, *19*, 1039.
(54) Becke, A. D. *J. Chem. Phys.* **1993**, *98*, 1372.
(55) Lee, C.; Yang, W.; Parr, R. G. *Phys. Rev. B* **1988**, *37*, 785.
(56) Zhang, Q.; Bell, R. L.; Truong, T. N. *J. Phys. Chem.* **1995**, *99*, 592.
(57) Maseras, F.; Morokuma, K. *J. Comput. Chem.* **1995**, *16*, 1170.
(58) Froese, R. D. J.; Morokuma, K. *Chem. Phys. Lett.* **1996**, *263*, 393.
(59) Froese, R. D. J.; Humbel, S.; Svensson, M.; Morokuma, K. *J. Phys. Chem. A* **1997**, *101*, 227.
(60) Humbel, S.; Sieber, S.; Morokuma, K. *J. Chem. Phys.* **1996**, *105*, 1959.
(61) Truhlar, D. G.; Garrett, B. C. *Acc. Chem. Res.* **1980**, *13*, 440.
(62) Truhlar, D. G.; Garrett, B. C. *Annu. Rev. Phys. Chem.* **1984**, *35*, 159.
(63) Truhlar, D. G.; Isaacson, A. D.; Garrett, B. C. In *Generalized transition state theory*; Truhlar, D. G., Isaacson, A. D., Garrett, B. C., Eds.; CRC Press: Boca Raton, FL, 1985; Vol. 4, p 65.
(64) Truong, T. N.; Truhlar, D. G. *J. Chem. Phys.* **1990**, *93*, 1761.
(65) Truhlar, D. G.; Isaacson, A. D.; Skodje, R. T.; Garrett, B. C. *J. Phys. Chem.* **1982**, *86*, 2252.
(66) Lu, D.-h.; Truong, T. N.; Melissas, V. S.; Lynch, G. C.; Liu, Y. P.; Garrett, B. C.; Steckler, R.; Isaacson, A. D.; Rai, S. N.; Hancock, G. C.; Lauderdale, J. G.; Joseph, T.; Truhlar, D. G. *Comput. Phys. Commun.* **1992**, *71*, 235.

particular, the transmission probability at energy E, $P(E)$, is given by

$$P(E) = \frac{1}{\{1 + e^{2\theta(E)}\}} \quad (5)$$

where $\theta(E)$ is the imaginary action integral evaluated along the tunneling path,

$$\theta(E) = \frac{2\pi}{h} \int_{s_l}^{s_r} \sqrt{2\mu_{eff}(s)|E - V_a(s)|}\, ds \quad (6)$$

and where the integration limits, s_l and s_r, are the reaction coordinate classical turning points. The reaction path curvature (i.e., corner-cutting) effect on the tunneling probability is included in the effective reduced mass, μ_{eff}. Thus, the ZCT transmission coefficients are obtained by setting μ_{eff} equal to μ in the above equation. Detailed descriptions of the VTST and tunneling methods are presented elsewhere.[61−63,65,66]

III. Computational Details. Electronic structure calculations were done at the BH&H-LYP level of theory[54,55] using the 6-31G(d,p) basis set unless otherwise specified. Geometries of all the stationary points were fully optimized without additional constraint beyond their symmetry ones. The reactant (trans-isomer) and intermediate (cis-isomer) geometries were optimized without any symmetry constraints. The transition-state geometries for the stepwise and concerted mechanisms were optimized with C_s and D_{2h} symmetry constraints, respectively. Normal-mode analyses confirm that stable structures, i.e., reactant and intermediate, have all real frequencies and the C_s transition state for the stepwise process has only one imaginary frequency, whereas the D_{2h} concerted transition state has two imaginary frequencies. The minimum energy path (MEP) calculations for the stepwise mechanism were performed in the mass-weighted Cartesian coordinate using the second-order Gonzalez and Schlegel method[67] with a sufficiently small step size of 0.05 amu$^{1/2}$ bohr. The MEP was followed for a total of 16 points in the direction of the reactant and for 13 points in the direction of the intermediate, for a total of 30 points including the transition state (TS). The MEP was then extrapolated to the reactant and intermediate. The locations of the equilibrium (reactant and intermediate) structures along the minimum energy path in the mass-weighted Cartesian coordinate were calculated following the method proposed by Zhixing.[68] For rate calculations, 15 Hessian grid points along the MEP were selected using the automated focusing technique.[53] The automated focusing technique uses a combination of the barrier shape and the second derivatives of the Z-matrix geometrical parameters to predict the regions along the MEP that are sensitive to rate calculation. As discussed below, the BH&H-LYP level of theory was found to yield the barrier slightly too high. To improve the energetic information of the stepwise mechanism, single-point energy calculations have been carried out using the recently proposed IMOMO method.[57−60] This method has been shown to provide rather accurate energetic information compared to full high-level calculations but at a significantly lower cost, particularly for large systems.[51] In these calculations, a small active subregion, that is most critical to the chemical process, is treated at the more accurate CCSD(T)/cc-pVDZ level of theory, while the remaining region is still at the BH&H/6-31G(d,p) level of theory. All electronic structure calculations were performed using the Gaussian 94 program.[69] The TST and CVT rate calculations were performed using our TheRate program.[53]

Results and Discussion

I. Equilibrium Structures. Full geometry optimization of the reactant (trans-isomer) leads to a D_{2h} structure. The calculated structure is depicted in Figure 2, and the geometrical parameters are displayed in Table 1. As can be seen from the table, the present calculated BH&H-LYP data agree well with those from calculations using LDA[35] and B3-LYP,[42] and from X-ray[1] data. The largest differences between our optimized structure and the X-ray data are 0.14 Å in bond lengths (N−H $r1$ bond) and 5.6° in angles (∠CNH a10 angle). However, it is well known that X-ray methods would not be able to locate

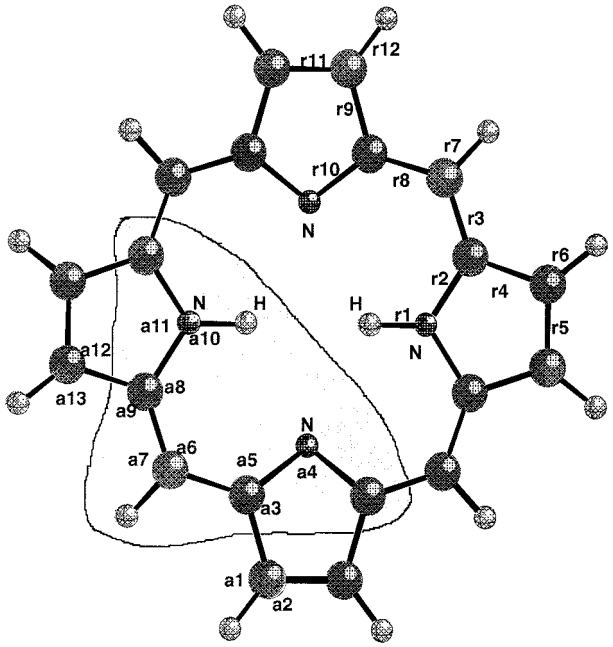

Figure 2. Geometry of the D_{2h} trans-isomer. See Table 1 for the calculated values of bond distances and bond angles. The shaded area shows the model system in the present IMOMO calculations that is treated at the CCSD(T)/cc-pVDZ level of theory, while the rest is treated at BH&H-LYP/6-31G(d,p) level.

Table 1. Calculated and Experimental Bond Distances and Bond Angles for the Trans-Isomer (D_{2h}) (Bond Distances Are in Angstroms and Bond Angles Are in Degrees)

bond length (r)/ bond angle (a)	this work	LDF[a]	B3-LYP/TZ2P[b]	X-ray[c]
r1	1.00	1.04	1.01	0.86
r2	1.36	1.36	1.37	1.38
r3	1.38	1.39	1.39	1.40
r4	1.43	1.42	1.43	1.43
r5	1.36	1.37	1.37	1.37
r6	1.07	1.09	–	1.14
r7	1.08	1.10	–	1.17
r8	1.39	1.39	1.39	1.37
r9	1.45	1.44	1.45	1.46
r10	1.35	1.36	1.36	1.38
r11	1.34	1.36	1.35	1.35
r12	1.07	1.10	–	1.02
a1	125.4	125.7	–	–
a2	128.5	128.2	–	–
a3	111.0	111.6	–	110.2
a4	105.7	104.6	105.8	105.9
a5	125.7	124.3	125.6	125.3
a6	126.8	127.6	127.1	126.7
a7	116.1	115.6	–	–
a8	125.8	125.3	125.6	124.8
a9	127.6	127.1	–	127.6
a10	124.6	125.1	125.6	130.2
a11	110.8	109.9	110.9	109.3
a12	107.9	107.5	–	108.2
a13	124.4	124.7	–	–

[a] Reference 35. [b] Reference 42. [c] Reference 1 (see Figure 2 for labels of bond lengths and angles).

(67) Gonzalez, C.; Schlegel, H. B. *J. Phys. Chem.* **1990**, *94*, 5523.
(68) Zhixing, C. *Theor. Chim. Acta* **1989**, *75*, 481.
(69) Frisch, M. J.; Trucks, G. W.; Schlegel, H. B.; Gill, P. M. W.; Johnson, B. G.; Robb, M. A.; Cheeseman, J. R.; Keith, T.; Petersson, G. A.; Montgomery, J. A.; Raghavachari, K.; Al-Laham, M. A.; Zakrzewski, V. G.; Ortiz, J. V.; Foresman, J. B.; Cioslowski, J.; Stefanov, B. B.; Nanayakkara, A.; Challacombe, M.; Peng, C. Y.; Ayala, P. Y.; Chen, W.; Wong, M. W.; Andres, J. L.; Replogle, E. S.; Gomperts, R.; Martin, R. L.; Fox, D. J.; Binkley, J. S.; Defrees, D. J.; Baker, J.; Stewart, J. P.; Head-Gordon, M.; Gonzalez, C.; Pople, J. A. *Gaussian 94, Revision D.3*; Gaussian Inc.: Pittsburgh, PA, 1994.

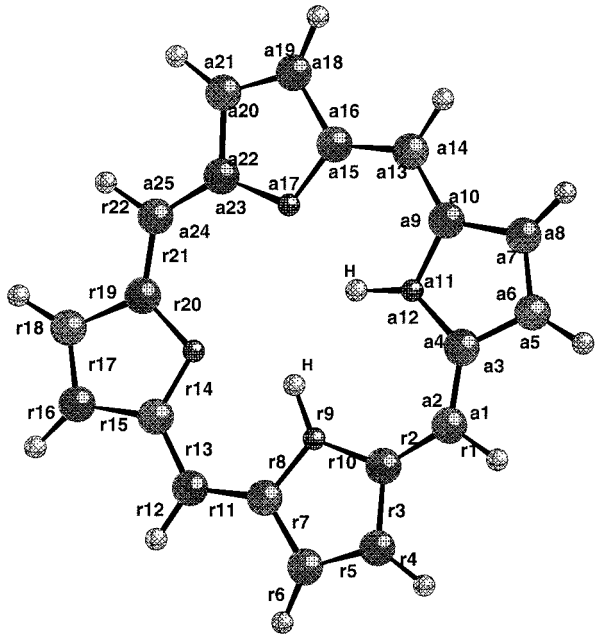

Figure 3. Geometry of the C_{2v} cis-isomer. See Table 2 for the calculated values of bond distances and bond angles.

hydrogen nuclei accurately, and the N−H bond distance of 0.86 Å estimated by the X-ray method is certainly too short compared to the normal N−H bond. Smaller differences of at the most 0.01 Å in bond lengths and 0.3° in bond angles are obtained when comparing the present results with those from B3-LYP/TZ2P[42] calculations. It is interesting to note that there are also small differences between the present BH&H-LYP and LDA results of Almlöf et al.[34] Similarly, the fully optimized geometry of the intermediate cis-isomer (see Figure 3 and Table 2) is very close to both the B3-LYP results of Baker et al.[42] and the MP2/DZP2 results of Almlöf et al.[34] with C_{2v} symmetry constraints. Note that the LDA geometry for the C_{2v} constrained intermediate from Ghosh and Almlöf[39] differs from the present BH&H-LYP one by less than 0.05 Å in bond distances and 3.6° in angles. This indicates that the stable structures are not very sensitive to the nonlocal characteristics of the DFT functionals. Our calculated BH&H-LYP frequencies for trans- and cis-isomers are given in Table 7 in the Appendix. The present calculated frequencies for trans-isomer are about 10% too large compared to the data from the scaled quantum mechanical (SQM) force field based on B3-LYP/6-31G(d) force constants.[41,70]

II. Transition-State Structures. The transition-state structures for the stepwise mechanism with marked bond lengths and angles are shown in Figure 4. The structure has been optimized with C_s symmetry constraints. Normal-mode analysis confirms this to be the correct saddle point with a single imaginary frequency of 1671*i* cm^{-1} whose eigenvector corresponds to distortion toward the reactant and intermediate. From Figure 4a, the transferring hydrogen atom lies closer to the accepting nitrogen by 0.04 Å, indicating that this transition state is closer to the intermediate structure, as intuitively predicted according to Hammond's postulate.[71] There are very small differences between the BH&H-LYP and B3-LYP geometries, particulaly within 0.01 Å in bond distances and 0.3° in bond angles.

The second-order transition-state structure of the concerted mechanism is shown in Figure 5, and the geometrical data are displayed in Table 3, along with the B3-LYP results from Baker et al.[42] These structures were optimized with D_{2h} symmetry constraints. The largest differences between the present calculated bond distances and bond angles compared to those obtained by Baker et al. are only 0.01 Å and 0.2°, respectively. Normal-mode analysis yields two imaginary frequencies of 1654*i* and 1562*i* cm^{-1} compared to those of 1853*i* and 1425*i* cm^{-1} from the B3-LYP/6-31G(d) level of theory. The eigenvector of the smaller imaginary frequency corresponds to motions of the two hydrogen atoms in the direction that connects the second-order saddle point and the cis-isomer, as denoted by path III in Figure 1. The larger imaginary frequency mode (1654*i* cm^{-1}) corresponds to synchronous motions of the two hydrogen atoms that connect the two trans-isomers, as denoted by path II in Figure 1. Our calculated BH&H-LYP frequencies for TS and second-order TS geometries are given in Table 7 in the Appendix.

Table 2. Calculated Bond Distances and Bond Angles for the Cis-Isomer (C_{2v}) (Bond Distances Are in Angstroms and Bond Angles Are in Degrees)

bond length (r)/ bond angle (a)	this work	LDF[a]	B3-LYP/TZ2P[b]
r1	1.07	1.10	–
r2	1.39	1.38	1.39
r3	1.43	1.43	1.43
r4	1.07	1.09	–
r5	1.36	1.37	1.37
r6	1.07	1.09	–
r7	1.42	1.42	1.43
r8	1.37	1.37	1.37
r9	1.01	1.06	1.02
r10	1.36	1.37	1.37
r11	1.38	1.39	1.39
r12	1.08	1.10	–
r13	1.39	1.39	1.40
r14	1.35	1.36	1.36
r15	1.45	1.44	1.45
r16	1.07	1.09	–
r17	1.34	1.36	1.35
r18	1.07	1.09	–
r19	1.46	1.44	1.46
r20	1.34	1.36	1.35
r21	1.39	1.39	1.40
r22	1.08	1.10	–
a1	114.7	114.8	–
a2	130.6	130.4	131.0
a3	125.0	123.7	–
a4	128.6	128.9	128.6
a5	124.0	123.7	–
a6	108.4	108.2	–
a7	107.7	107.3	–
a8	127.6	128.6	–
a9	123.6	122.5	123.3
a10	129.5	129.7	–
a11	110.7	109.5	110.7
a12	131.6	135.2	132.0
a13	124.0	123.4	124.2
a14	117.4	117.8	–
a15	123.3	122.5	123.1
a16	125.7	126.0	–
a17	106.3	105.5	106.3
a18	125.7	125.4	–
a19	128.5	128.9	–
a20	106.5	106.7	–
a21	128.3	128.8	–
a22	110.4	110.7	–
a23	127.2	127.2	127.1
a24	115.0	115.1	–
a25	130.0	129.8	130.4

[a] Reference 35. [b] Reference 42 (see Figure 3 for labels of bond lengths and angles).

(70) Kozlowski, P. M.; Jarzecki, A. A.; Pulay, P.; Li, X.; Zgierski *J. Phys. Chem.* **1996**, *100*, 13985.

(71) Hammond, G. S. *J. Am. Chem. Soc.* **1955**, *77*, 334.

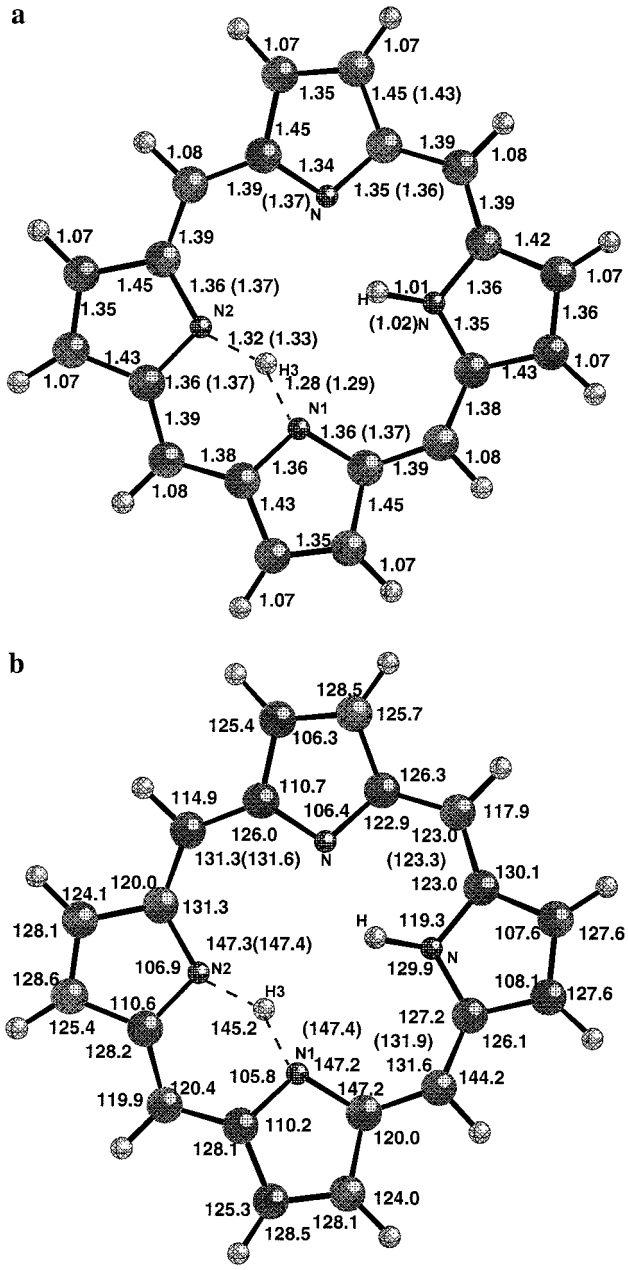

Figure 4. Calculated geometry of the C_s transition state (a) bond lengths (Å) and (b) bond angles (degrees) for the stepwise mechanism. The values in the parentheses show the calculated data from Baker et al. (ref. 42).

III. Energetics. The calculated reaction energetic information along with previous theoretical and experimental results is listed in Table 4. The calculated energy difference between the reactant (trans-isomer) and intermediate (cis-isomer) is 9.1 kcal/mol. This value is reduced by only 0.4 kcal/mol when the zero-point energy correction is included. The present result is within previous MP2 results of 7.6−10.0 kcal/mol and is 0.8 kcal/mol larger than the B3-LYP value. The classical barrier height for the trans ↔ cis tautomerization process in the stepwise mechanism is predicted to be 18.6 kcal/mol at the BH&H-LYP level. This is about 2 kcal/mol too large compared to the MP2 and B3-LYP results. It is also about 2 kcal/mol above the upper limit of the experimental estimate range for the classical barrier height of 12.6−16.3 kcal/mol from a laser-induced fluorescence spectroscopic measurement coupled with one-dimensional tunneling model.[18] To get a more reliable estimation of the barrier height, single-point energy calculations were performed at

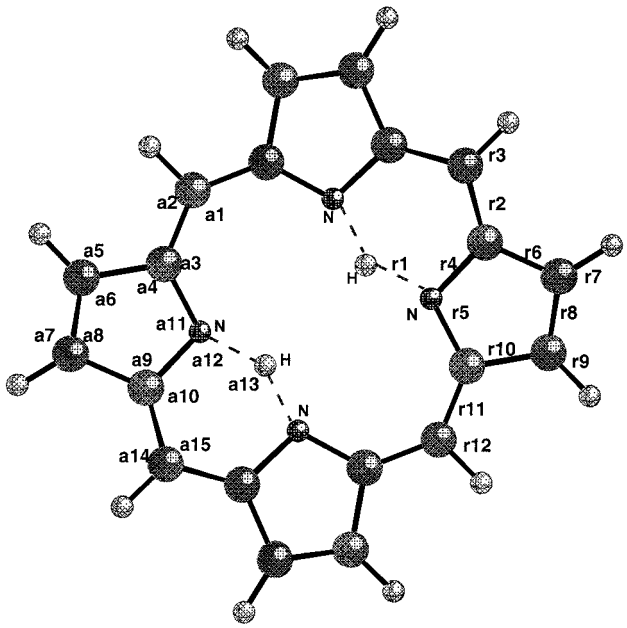

Figure 5. Geometry of the D_{2h} second-order transition state. See Table 3 for the calculated values of bond distances and bond angles.

Table 3. Calculated Bond Distances and Bond Angles for the Second-Order Saddle Point Structure (D_{2h}) (Bond Distances Are in Angstroms and Bond Angles Are in Degrees)

bond length (r)/ bond angle (a)	this work	B3-LYP/TZ2P[a]
r1	1.28	1.30
r2	1.39	1.39
r3	1.08	−
r4	1.36	1.37
r5	1.35	1.36
r6	1.43	1.43
r7	1.07	−
r8	1.35	1.36
r9	1.07	−
r10	1.44	1.45
r11	1.39	1.39
r12	1.08	−
a1	132.9	133.1
a2	113.6	−
a3	130.0	129.8
a4	108.7	−
a5	124.3	−
a6	107.7	−
a7	128.4	−
a8	106.2	−
a9	110.0	−
a10	121.0	120.9
a11	107.4	107.5
a12	106.8	106.5
a13	144.6	−
a14	120.0	−
a15	120.0	120.5

[a] Reference 42 (see Figure 5 for labels of bond lengths and angles).

CCSD(T)/cc-pVDZ level of theory for the shaded portions (see Figure 2) of the stationary point geometries using the IMOMO approach. The remaining part of the structures is treated at the BH&H-LYP/6-31G(d,p) level of theory. This resulted in a classical barrier height of 16.9 kcal/mol and a reaction energy difference of 8.2 kcal/mol. The IMOMO barrier height is in good agreement with the MP2 and B3-LYP results and the experimental estimate. The IMOMO barrier height for the cis ↔ trans tautomerization process is calculated to be 8.7 kcal/mol, versus 9.5 kcal/mol from the full calculation at the BH&H-

Table 4. Calculated Reaction Energy ΔE, Classical Barrier Height $\Delta V^{\ddagger}$, and Zero-Point Energy-Corrected Barrier Height ΔV_a for Inner Hydrogen Atom-Transfer Process in Free Base Porphyrin (in kcal/mol)

study	ΔE	$\Delta V^{\ddagger}$	ΔV_a
semiempirical[a]	8.9		
MP2/DZP//RHF SCF/DZP[b]	10.0		
MP2//LDF[c]	7.6		
B3-LYP/TZ2P[d]	8.3		
BH&H-LYP/6-31G(d,p)[e]	9.1		
IMOMO(CCSD(T):BH&H-LYP)[e]	8.2		
Stepwise Mechanism			
trans → TS			
Butenhoff and Moore[f]		12.6−16.3[g]	
MP2/DZP//RHF SCF/DZP[b]		16.7	
B3-LYP/TZ2P[d]		16.2	13.1
BH&H-LYP/6-31G(d,p)[e]		18.6	15.6
IMOMO(CCSD(T):BH&H-LYP)[e]		16.9	
cis → TS			
B3-LYP/TZ2P[d]		9.9	5.0
BH&H-LYP/6-31G(d,p)[e]		9.5	6.8
IMOMO(CCSD(T):BH&H-LYP)[e]		8.7	
Concerted Mechanism			
trans → TS			
MP2/DZP//RHF SCF/DZP[b]		19.3	
B3-LYP/TZ2P[d]		24.4	18.3
BH&H-LYP/6-31G(d,p)[e]		21.6	17.1

[a] Reference 28. [b] Reference 38. [c] Reference 39. [d] Reference 42. [e] This work. [f] Reference 18. [g] This is an experimental study.

Table 5. Comparison of Calculated BH&H-LYP/6-31G(d,p) Reaction Energies ΔE and Classical Barrier Heights $\Delta V^{\ddagger}$ (kcal/mol) in the Gas Phase and in Different Solvents for the NH Tautomerization Process in Free Base Porphyrin

solvent	ΔE	$\Delta V^{\ddagger}$
gas phase	9.1	18.6
heptane	9.5	18.9
toluene	9.0	18.8
ethanol	8.6	19.7

LYP/6-31G(d,p) level of theory. The BH&H-LYP reverse classical barrier height is found to agree well with the B3-LYP result of 9.9 kcal/mol. However, the classical barrier height for the concerted mechanism is calculated to be smaller by ∼3 kcal/mol. In contrast to the energy difference between reactant and intermediate, the zero-point energy correction was found to lower than the classical barriers in both mechanisms by about 3 kcal/mol and is significant.

To obtain an estimate for the solvent effects on the reaction energetics, we performed single-point calculations of porphyrin in different solvents using the polarizable continuum model (PCM).[72] In particular, heptane (dielectric constant, $\epsilon = 1.92$), toluene ($\epsilon = 2.38$), and ethanol ($\epsilon = 24.55$) were chosen for such calculations as these solvents were often used in experimental studies. The calculated reaction energy difference between the trans- and cis-isomers and classical barrier heights are listed in Table 5. For nonpolar solvents such as heptane and toluene, solvent effects are negligible. The effect is slightly larger for polar solvents such as ethanol. Note that the barrier height is increased by 1 kcal/mol in ethanol. This increase is due to smaller interactions between the transition-state and solvent molecules as compared to those of the reactant, where there exist weak hydrogen bonds between ethanol and the lone pairs of nitrogen atoms in the trans-isomer. These results are consistent with the earlier experimental report on the solvent

(72) Cossi, M.; Barone, V.; Cammi, R.; Tomasi, J. *Chem. Phys. Lett.* **1996**, *255*, 327.

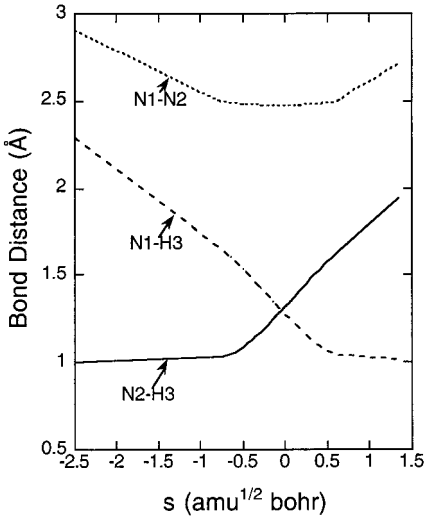

Figure 6. Selected bond distances along the minimum energy path plotted vs the reaction coordinate s in the mass-weighted Cartesian coordinate (see Figure 4 for bond labels).

independence of rate of intramolecular hydrogen atom transfer in free base porphyrin.[3] It has also been observed from liquid- and solid-state NMR studies that this NH tautomerization behavior is the same in liquid solution and in bulk solid, indicating the absence of medium influence.[15] This also implies that gas-phase calculations are probably sufficient to study the inner hydrogen-transfer process in the free base porphyrin system, as mentioned earlier.

IV. Minimum Energy Path. Here we examine the structural changes of porphyrin as it proceeds from the reactant to the intermediate on the stepwise path. The only significant change that is larger than 2% in the bond length is that of the transferring hydrogen atom. The N−H bond of the transferring hydrogen atom is lengthened by 32% to reach the transition-state structure (∼1.32 Å) from the reactant (∼1.00 Å). The angle labeled a10 in Figure 2 was found to have the largest change of −15.1% to reach the transition state (105.8°) from the reactant (124.6°). These active bond lengths and angles essentially relate to the N−H stretching and bending modes which were thought to be responsible for the process of tautomerization in mode-selective vibrational spectroscopic studies.[20] More detailed information on structural changes can be obtained from a plot of the donor−acceptor N−N and active N−H bond distances versus the reaction coordinate, as shown in Figure 6. Examination of N−N and N−H bond distance profiles as functions of the reaction coordinate reveals an interesting observation. In particular, the trans ↔ cis tautomerization process can be viewed as a two-stage process in which the changes in the structure along the reaction coordinate can be divided into two distinct parts, each involving different types of motions. Note that this is different from a two-step process which involves a stable intermediate. More specifically, the donor−acceptor N−N bond distance (N1−N2 bond as shown in Figure 4) first shortens from 2.91 to 2.51 Å, while the breaking N−H bond distance (N2−H3 bond as shown in Figure 4) remains relatively unchanged approximately up to $s = -0.8$ amu$^{1/2}$ bohr from the reactant. At this point, the N−N bond distance stays relatively constant while the hydrogen atom transfers from one N center to the other as its bond length is stretched from 1.0 to 1.32 Å to reach the saddle point. One can think of this two-stage process as the porphyrin first going through a global structure compression to bring the donor and acceptor sites closer together, so as to shorten the hydrogen atom-transfer path, thus lowering the

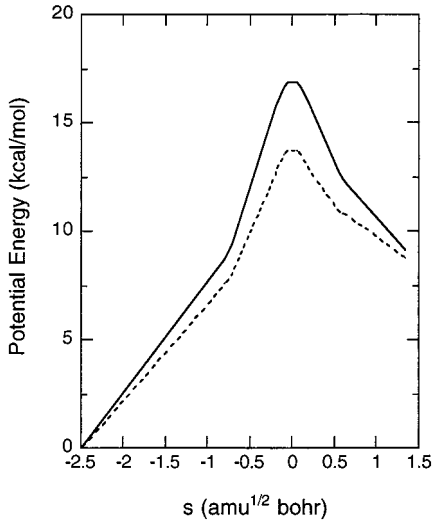

Figure 7. Classical potential energy $V_{MEP}(s)$ (solid line) and the vibrationally ground-state adiabatic potential energy $V_a^G(s)$ (dashed line) (kcal/mol) curves along the minimum energy path plotted vs the reaction coordinate s in the mass-weighted Cartesian coordinate.

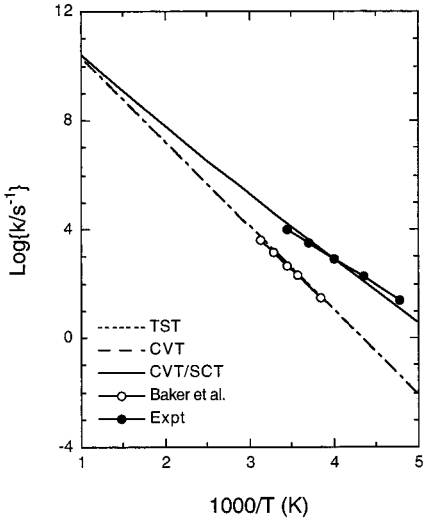

Figure 8. Comparison of Arrhenius plots of the experimental and calculated forward (trans-isomer → cis-isomer) rate constants vs 1000/T at different levels of theory for rate calculations and tunneling corrections. Note that the TST and CVT rate curves are overlapped. The experimental data are generated from the Arrhenius equation suggested in ref 15.

barrier. Such deformation will reach a point at which further compression would outcost the hydrogen atom-transfer process. At that point one observes solely hydrogen atom-transfer motion with no further global structure compression. Figure 7 shows the energy cost for global compression to be about 8.7 kcal/mol (the potential energy value at $s = -0.8$ amu$^{1/2}$ bohr). The remaining energy cost of ~8.2 kcal/mol can be thought of as the barrier to hydrogen atom transfer in the second stage. Such a two-stage process observed here is not unique to this tautomerization process. We have also observed the same structural changes in the concerted double hydrogen atom transfers in formamidine−water and formamide−water complexes.[43,44] This information could be very useful in designing new porphyrins for materials science and biological applications. Previously, there has been some theoretical[73,74] and experimental[75,76] discussion on the structural changes of the porphyrin skeleton on hydrogen atom migration in the case of monodeprotonated free base porphyrin. However, the theoretical discussions were limited to the differences between the reactant and transition-state structures and thus were not able to reveal the two-stage process as discussed above.

V. Kinetics. Transition-state theory (TST) and canonical variational transition-state theory (CVT) rate calculations including different tunneling contributions were carried out for the trans ↔ cis isomerization process in free base porphyrin in the temperature range of 200−1000 K on the IMOMO single-point energy corrected potential energy surface. Figure 8 displays the Arrhenius plot of the calculated results at different levels of theory for the forward reaction of trans ↔ cis isomerization. Recrossing effect on the gas-phase potential surface was found to be very small, as expected due to the relatively large barrier height. Note that recrossing due to collisions with solvent molecules is not included in the present calculations. However, it is expected to be small due to the observed small solvent effects, even within a polar solvent such as methanol. Tunneling effects were found to be significant, particularly in the lower temperature range, as indicated by the curvature of the CVT/SCT curve and its large deviation from the CVT results. For example, at 200 K, tunneling enhances the transfer rate by a factor of about 410. A previous theoretical rate calculation done by Baker et al.[42] was performed at a simple TST level of theory without incorporating any tunneling corrections. Consequently, the results of Baker et al. were found to be lower by a factor of 60 compared to the available experimental value of 1.8e + 3 s^{-1} at 260 K from Braun et al.[15] Our most accurate results for the rate constants, namely the canonical variation TST with multidimensional semiclassical small-curvature tunneling approximation (CVT/SCT), are in excellent agreement with the available experimental data. Since the present IMOMO-corrected potential surface is similar to the B3-LYP one, TST rate constants from both surfaces are similar (see Figure 8). It is interesting to point out that the SCT transmission coefficient at 260 K is 60. This indicates that the error in the TST results of Baker et al. is mainly due to not including tunneling effects. The non-Arrhenius equation for the forward NH tautomerization process (the first step of the process) in free base porphyrin is k (s^{-1}) = 5.05e + 08$T^{1.29}$ exp(−9.9 kcal mol^{-1}/RT) in the temperature range of 200−1000 K from the best fit to the calculated CVT/SCT rate data.

Calculated activation energies (E_a) in the temperature range of 200−300 K for NH tautomerization along with available experimental data are listed in Table 6. Notice first that the CVT/SCT calculated activation energy of 10.8 kcal/mol is within the range of experimental data of 9.0−11.4 kcal/mol from Eaton and co-workers[3] and higher than that of 8.8 kcal/mol from Braun and co-workers.[15] There is a larger uncertainty in the experimental activation energy at very low temperatures. Particularly, the activation energy of 4.8−5.6 kcal/mol at 110 K from laser-induced fluorescence spectroscopy experiments reported by Butenhoff and Moore[18] is much lower than the value of 8.3 kcal/mol from Frydman et al. at the same temperature. The present TST activation energy of 14.1 kcal/mol is slightly higher that that of 13.3 kcal/mol from TST calculations of Baker and co-workers. This is mostly due to the classical barrier used in the present calculations being 0.7 kcal/mol higher (see Table 4). When tunneling corrections are included, the calculated E_a improves as a more accurate tunneling method is employed.

(73) Vangberg, T.; Ghosh, A. *J. Phys. Chem. B* **1997**, *101*, 1496.
(74) Brackhagen, O.; Scheurer, C.; Meyer, R.; Limbach, H. *Ber. Bunsen-Ges. Phys. Chem.* **1998**, *102*, 303.
(75) Braun, J.; Hasenfratz, C.; Schwesinger, R.; Limbach, H. *Angew. Chem., Int. Ed. Engl.* **1994**, *33*, 2215.
(76) Braun, J.; Schwesinger, R.; Williams, P. G.; Morimoto, H.; Wemmer, D. E.; Limbach, H.-H. *J. Am. Chem. Soc.* **1996**, *118*, 11101.

Table 6. Comparison of Experimental and Calculated Energy of Activation E_a (in kcal/mol) for the NH Tautomerization Process in Free Base Porphyrin Following Different Methods of Rate Calculation and Tunneling Correction

method	E_a
experimental	
Abraham et al.[a]	9.2 (308 K)
Eaton and Eaton[b]	9.0−11.4 (298 K)
Braun et al.[c]	8.8 (209−309 K)
	9.3 (223−290 K)
Frydman et al.[d]	8.3 (110 K)
Butenhoff and Moore[e]	4.8−5.6 (110 K)
theory (200−300 K)	
TST	14.1
TST/W	13.3
TST/Eckart	11.1
CVT	14.1
CVT/ZCT	11.6
CVT/SCT	10.8

[a] Reference 2. [b] Reference 3; this is for tetraaryl porphyrin. [c] Reference 15; the value in the lower line is for the bulk solid. [d] Reference 17. [e] Reference 18.

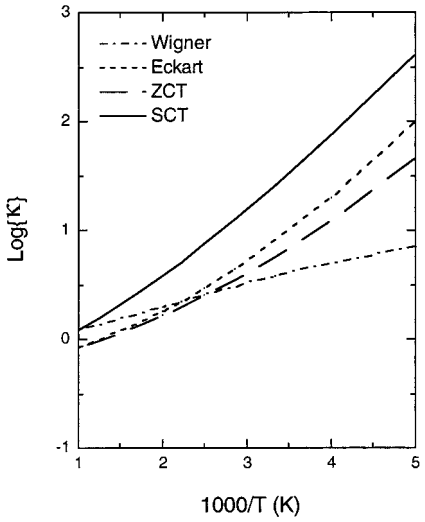

Figure 9. Log plot of calculated transmission coefficient (κ) vs 1000/T using different tunneling models.

Due to the importance of tunneling in this process, it is worthwhile to examine the performance of different tunneling approximations considered here. Figure 9 displays the calculated transmission coefficient (κ) as a function of the temperature using different tunneling models. The SCT method is the most accurate approximation used in this study, and thus we used it as a reference point for comparison. First, the Wigner model, as expected, greatly underestimates the tunneling contribution since it assumes tunneling to occur mostly at the top of the barrier. It is reasonable only at moderate to high temperatures. Even though the Eckart model requires only potential information at the stationary points (reactant, transition state, and product), it predicts a much more accurate tunneling contribution than the Wigner model, which needs information only at the reactant and transition state. Recall that in the Eckart model, the reaction path curvature effect is not included, and the vibrationally ground-state adiabatic potential energy curve for tunneling is approximated by a one-dimensional Eckart function. Thus, it is an approximation to the zero curvature tunneling (ZCT) method. A remarkable agreement between results from the Eckart model and the ZCT method indicates the potential curve along the MEP can be well represented by an Eckart function. Our results suggest that the Eckart tunneling model should be used in experimental analysis, as was done by

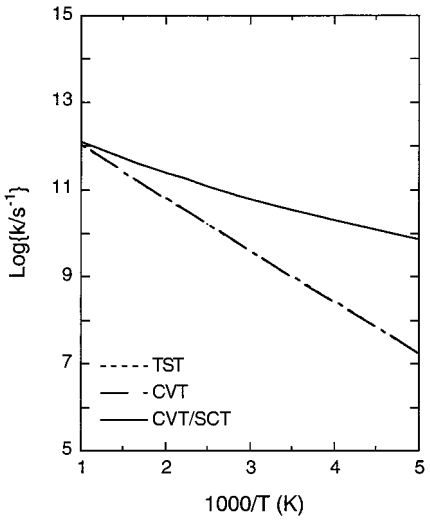

Figure 10. Arrhenius plots of the calculated reverse (trans-isomer → cis-isomer) rate constants vs 1000/T at different levels of theory for rate calculations and tunneling corrections. Note that the TST and CVT rate profiles are overlapped.

Butenhoff and Moore.[18] Finally, comparing the ZCT and SCT results, we found that the "corner-cutting" effect accounts for nearly an order of magnitude increase in the rate for temperatures below 300 K.

Figure 10 depicts the Arrhenius plot of the calculated results for the reverse trans ↔ cis NH tautomerization process, which is essentially the second step of the stepwise path. The recrossing effect was also found to be very small. Again, very large tunneling effects were found in the lower temperature range. The activation energy (E_a) for this process was calculated to be 2.1 kcal/mol in the temperature range of 200−300 K from the present CVT/SCT rate calculations. The non-Arrhenius equation for reverse NH tautomerization process (the second step of the process) in free base porphyrin is k (s^{-1}) = 9.71e + 08$T^{1.17}$ exp(−1.7 kcal mol^{-1}/RT) over the temperature range of 200−1000 K from the best fit to the calculated CVT/SCT rate data. Previously there has been some discussion regarding the lifetime of the cis-isomer, as to whether it can be experimentally detected. According to our CVT/SCT data for cis → trans conversion, the lifetime of the cis-isomer is calculated to be ∼25 ps, versus ∼30 μs for the trans-isomer. The presently calculated lifetime for the cis-isomer is substantially shorter than the previous estimation of 1−10 ns.[14,42] However, the previous results are based on methods that did not apply any appropriate tunneling corrections. Thus, the present results using the CVT/SCT method would be more reliable.

Conclusions

We have presented a direct ab initio dynamics study on the kinetics of the NH tautomerization process in free base porphyrin. This study provides a detailed examination of the mechanism of this reaction and the importance of quantum mechanical tunneling and solvent effects. We found that the double hydrogen atom-transfer process prefers a stepwise mechanism that is consistent with experimental observations. Detailed analysis reveals that this migration consists of two separate types of motion, referred to as a two-stage process in this study. In the first stage, the porphyrin ring goes through a global structural deformation in attempting to bring the donor and acceptor sites closer together to make the local hydrogen atom-transfer process possible in the second stage. This deformation accounts for nearly 50% of the total activation

Table 7. Calculated BH&H-LYP/6-31G(d,p) Frequencies for Different Stationary Point Geometries of Free Base Porphyrin

geometry	frequency
trans	3754, 3704, 3363, 3363, 3351, 3351, 3345, 3345, 3329, 3329, 3296, 3296, 3296, 3296, 1724, 1713, 1706, 1681, 1662, 1640, 1620, 1610, 1610, 1607, 1548, 1525, 1509, 1504, 1503, 1492, 1457, 1453, 1441, 1424, 1373, 1331, 1319, 1310, 1271, 1259, 1238, 1227, 1223, 1188, 1132, 1127, 1122, 1092, 1075, 1053, 1051, 1051, 1042, 1017, 1008, 978, 977, 975, 972, 968, 920, 911, 908, 899, 850, 847, 837, 835, 831, 827, 821, 806, 787, 781, 768, 762, 747, 745, 745, 740, 727, 721, 707, 704, 687, 659, 503, 463, 449, 435, 409, 371, 371, 352, 327, 322, 313, 305, 220, 217, 196, 161, 139, 130, 110, 98, 70, 58
cis	3555, 3514, 3363, 3363, 3350, 3350, 3345, 3345, 3329, 3328, 3304, 3304, 3298, 3273, 1740, 1716, 1695, 1676, 1657, 1641, 1632, 1627, 1604, 1556, 1555, 1528, 1524, 1501, 1499, 1480, 1476, 1460, 1444, 1423, 1377, 1365, 1346, 1291, 1268, 1265, 1244, 1234, 1222, 1188, 1133, 1126, 1120, 1095, 1090, 1070, 1064, 1053, 1026, 1018, 1005, 985, 977, 974, 973, 968, 936, 910, 907, 890, 858, 855, 842, 835, 833, 832, 822, 809, 794, 782, 769, 756, 752, 751, 739, 729, 726, 716, 711, 702, 692, 634, 503, 457, 455, 435, 416, 382, 360, 351, 330, 328, 321, 313, 212, 202, 197, 165, 154, 143, 114, 96, 71, 58
TS	3539, 3363, 3358, 3357, 3351, 3345, 3337, 3336, 3329, 3319, 3307, 3290, 3278, 1950, 1733, 1717, 1680, 1669, 1655, 1645, 1630, 1620, 1606, 1569, 1556, 1538, 1524, 1505, 1495, 1476, 1463, 1451, 1442, 1395, 1380, 1352, 1296, 1275, 1263, 1258, 1238, 1231, 1226, 1217, 1141, 1129, 1124, 1118, 1103, 1075, 1070, 1062, 1051, 1044, 1019, 1009, 978, 974, 972, 967, 926, 910, 902, 889, 859, 848, 842, 841, 832, 826, 820, 817, 797, 787, 770, 763, 752, 749, 743, 740, 728, 722, 709, 705, 690, 502, 460, 453, 442, 439, 422, 385, 360, 351, 339, 331, 312, 236, 207, 194, 185, 160, 156, 134, 99, 61, 56, 1671*i*
second-order TS	3358, 3358, 3358, 3358, 3337, 3337, 3337, 3337, 3319, 3319, 3281, 3281, 1980, 1936, 1737, 1682, 1678, 1661, 1661, 1634, 1630, 1622, 1597, 1565, 1558, 1544, 1530, 1514, 1481, 1472, 1462, 1445, 1425, 1399, 1365, 1297, 1279, 1272, 1272, 1272, 1259, 1231, 1222, 1216, 1164, 1130, 1124, 1122, 1118, 1098, 1079, 1074, 1064, 1055, 1044, 1033, 977, 974, 973, 968, 922, 916, 898, 892, 864, 848, 843, 835, 834, 827, 819, 816, 807, 777, 767, 764, 747, 746, 739, 733, 723, 711, 707, 702, 502, 460, 456, 455, 453, 444, 394, 391, 366, 353, 348, 312, 236, 216, 205, 205, 172, 162, 136, 108, 57, 56, 1562*i*, 1654*i*

energy. Solvent effects as modeled by a dielectric continuum method were found to be small and are in agreement with experimental observations. Thermal rate constants for this tautomerization process were calculated using a full canonical variational transition-state theory augmented by several tunneling approximations. We found that the tunneling effect is significant. The calculated rate constants and activation energy for the NH tautomerization (trans-isomer → cis-isomer) process are in good agreement with the available experimental data. These results indicate that the computational methodology used in this study is sufficiently accurate for modeling the kinetics of the NH tautomerization processes in porphyrins. It would be interesting and challenging to the computational method presented here to also study the kinetic isotope effects for these processes. Such a study will be presented in a forthcoming paper.

Acknowledgment. This work is supported by the National Science Foundation. An allocation of computer time from the University of Utah Center for High Performance Computing is gratefully acknowledged.

JA9925094